Article

Deciphering Reaction Network for the Switchable Production of Tetrahydroquinoline or Quinoline with MOF-Supported Pd Tandem Catalysts

Long Qi, Jingwen Chen, Biying Zhang, Renfeng Nie, Zhiyuan Qi, Takeshi Kobayashi, Zongbi Bao, Qiwei Yang, Qilong Ren, Qi Sun, Zhiguo Zhang, and Wenyu Huang

ACS Catal., **Just Accepted Manuscript** • DOI: 10.1021/acscatal.0c00899 • Publication Date (Web): 17 Mar 2020

Deciphering Reaction Network for the Switchable Production of Tetrahydroquinoline or Quinoline with MOF-Supported Pd Tandem Catalysts

Long Qi,[a,‡,*] Jingwen Chen,[b,c,‡] Biying Zhang,[b] Renfeng Nie,[b] Zhiyuan Qi,[b] Takeshi Kobayashi,[a] Zongbi Bao,[c] Qiwei Yang,[c] Qilong Ren,[c] Qi Sun,[c] Zhiguo Zhang,[c,*] Wenyu Huang[a,b,*]

[a] U.S. DOE Ames Laboratory, Iowa State University, Ames, Iowa 50010, USA

[b] Department of Chemistry, Iowa State University, Ames, Iowa 50010, USA

[c] Key Laboratory of Biomass Chemical Engineering of Ministry of Education, College of Chemical and Biological Engineering, Zhejiang University, Hangzhou 310027, China

KEYWORDS: tandem catalysis, reaction network, metal-organic frameworks, metal nanoparticles, operando spectroscopy, mechanistic study.

ABSTRACT: Mechanistic study of heterogeneous tandem catalytic system is crucial, but remains challenging, for the understanding and improving catalyst activity and selectivity. Here, we demonstrate that a thorough mechanistic study of a multistep reaction can guide us to the controllable selective synthesis of phenyltetrahydroquinoline or phenylquinoline with easily accessible precursors. The one-pot production can be achieved, catalyzed by a well-defined, bifunctional metal-organic framework-supported Pd nanoparticles, with only water as the side product. Our mechanistic study identifies six transient intermediates and ten transformation steps from the operando magic angle spinning NMR study under 27.6 bar H_2. In particular, reactive intermediate 2-phenyl-3,4-dihydroquinoline cannot be observed with conventional chromatographic techniques but is found to reach the maximal concentration of 0.11 mol L^{-1} under the operando condition. The most probable reaction network is further deduced based on the kinetic information of reaction species, obtained from both operando and *ex situ* reaction studies. This deep understanding of the complex reaction network enables the kinetic control of the conversions of key intermediate, 2-phenyl-3,4-dihydroquinoline, with the addition of a homogeneous co-catalyst, allowing the selective production of tetrahydroquinoline or quinoline on demand. The demonstrated methods in this work open up new avenues towards efficient modulation of reactions with complex network to achieve desired selectivities.

INTRODUCTION

The concept of tandem catalysis, whereby sequential chemical conversions catalyzed by multiple active sites in one pot give desirable product selectively, has gained significant interest for the selective catalytic production of chemicals and fuels.[1] This interest is based on the prospects of boosting the atom economy, as costly intermediate separations and purification processes could be avoided. Identified among the 5 priority research directions for catalysis science by U.S. DOE in 2017,[2] a significant challenge is how to direct convoluted transformations through the desired routes for the target product in a complexed reaction network, given that tandem catalysis typically involves multiple transiently-evolved intermediates. Thus far, optimization of reaction conditions has relied mainly on laborious and time-consuming trial-and-error experiments. The establishment of complex reaction networks, including reactants, intermediates, and favored and unwanted products, would help to elucidate the underlying principles of such transformations and, in turn, guide the design of efficient catalytic systems.

Probing the reaction network requires but is not limited to: (1) identifying reaction species, (2) deconvoluting individual reaction paths, and (3) understanding the reversibility and rates of interconversions. However, due to the co-presence of solid catalysts, reaction solution, and reactive gas, an in-depth study of heterogeneous tandem reactions and the associated complexed reaction network is rather challenging, in particular when intermediates are unstable upon sampling. Even for stable species, the limited number of intermittent sampling at

high temperature and pressure greatly restricts the data density to delineate the reaction network accurately.

Advanced techniques as noteworthy as *operando* magic angle spinning NMR spectroscopy (MAS-NMR)[3] has proven to be unique for detailed structural and kinetic information of multiphasic systems at both high temperatures and high pressures.[4,5] Accordingly, *operando* MAS-NMR techniques provide the opportunity for monitoring the reaction intermediates and ultimately mapping out the reaction networks. To elaborate the feasibility of our plan, we choose a model tandem catalytic system for the production of tetrahydroquinoline (THQ) or quinoline, where the first chemical conversion is the Claisen-Schmidt condensation of 2-nitrobenzaldehyde (NBA) and acetophenone (ACP) to nitrochalcone, followed by its reductive intramolecular cyclization, Scheme 1. This reaction is ideal not only because the production of THQ and quinoline architectures, widely existing in bioactive natural products,[6] can serve as key pharmaceutical ingredients,[7-13] and THQ is essential building block of hydrogen-storage materials,[14-16] but also due to the involvement of multiple transiently-evolved intermediates as a result of the concurrent reduction of several functionalities (i.e., -NO_2, C=C, C=O, C=N, and arenes) during reductive cyclization.

In order to thoroughly study this tandem reaction and gain insights into the fundamental principles behind, a stable, well-defined catalyst is necessary. Metal-organic frameworks (MOFs) give great promises for the integration of multiple active species for tandem catalysis. By judiciously selecting the metal centers/clusters and ligands of the MOF, a microenvironment is created, which can be used to introduce other catalytic species further and to aid the catalytic process. Considering that active species with acidity and hydrogenation capability are needed to accomplish the aforementioned transformations, we constructed a bifunctional catalyst by supporting Pd nanoparticles (NPs) on an acidic metal-organic framework (MOF), Pd/UiO-66, Scheme 1. Using the advanced *operando* spectroscopic method, we detected and quantified key intermediates (under 27.6 bar H_2 at 40°C), in particular, the reactive 2-phenyl-3,4-dihydroquinoline and (*E*)-3-(2-(hydroxyamino)phenyl)-1-phenylprop-2-en-1-one that cannot be detected by *ex-situ* sampling methods. Significantly, the obtained mechanistic information was then utilized to unravel the high selectivity in the phenyltetrahydroquinoline (PTHQ) synthesis for the Pd/UiO-66 catalyst. More importantly, the mechanistic insights further allowed us to switch the selectivity of the product between PTHQ and phenylquinoline (PQ) by adding a co-catalyst. These results provide a new insight for manipulating complex transformations.

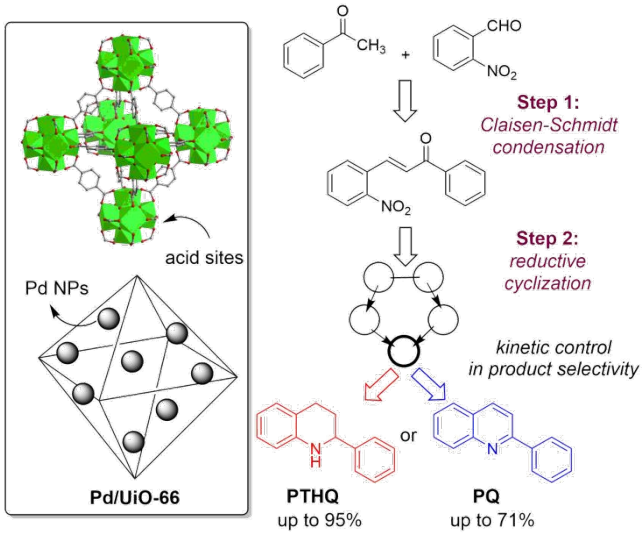

Scheme 1. Kinetic control in the selective synthesis of PTHQ and PQ catalyzed by Pd/UiO-66.

RESULTS AND DISCUSSION

Production of PTHQ with bifunctional Pd/UiO-66 MOFs have attracted great attention as solid acid catalysts.[17-20] Modifying the organic linkers or immobilizing metal nanoparticles also introduces other active sites.[21-23] The co-existence of different active sites can enable tandem catalysis of two or more consecutive steps in one pot to eliminate unnecessary separation/purification steps and boost atom economy.[1,24]

In the multistep synthesis of PTHQ (Scheme 1), we first carried out the Claisen-Schmidt condensation between ACP (***1***) and NBA (***2***) at 100 °C with three different acidic MOFs, including UiO-66(Zr), HKUST(Cu), and MIL-101(Cr). The structural characterization results of these three MOFs are shown in Figures S1-S2. UiO-66 shows the highest catalytic activities achieving quantitative yield of *ortho*-nitrochalcone (***4***) in 3 h, Figure 1. The high activity could be owing to the combined efforts of Lewis acidic Zr with missing ligand and Brønsted site by the μ_3-OH in the SBU.[25,26] The strong Lewis acidity has been demonstrated in the Meerwein - Ponndorf - Verley (MPV) reduction of prenol and furfural.[27] MIL-101 with coordination-unsaturated Cr sites show only 8% conversion in 3 h, which is much less active compared to UiO-66. Lewis acidic HKUST-1 is inefficient in promoting the condensation reaction, although it is active in catalyzing the Friedländer reaction for the synthesis of quinoline.[28] In comparison, an inorganic solid acid, γ-Al_2O_3, was examined and found nearly inactive as well. Therefore, UiO-66 is chosen as the acidic catalyst for the multistep reaction.

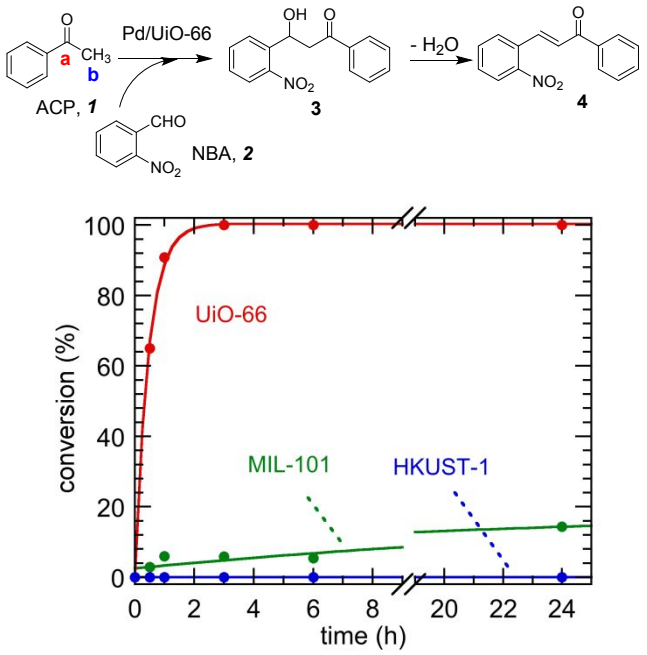

Figure 1. Conversion of NBA versus reaction time for the MOF-catalyzed Claisen-Schmidt condensation reaction. Reaction conditions: NBA (0.2 mmol), ACP (0.4 mmol), catalyst (5 mg), toluene (1 mL), 100 °C. The lines are added only to guide the eye.

To introduce hydrogenation capability to the MOF, we synthesized Pd NPs supported on UiO-66 *via* wetness impregnation followed by reduction under flowing H_2.[29] The powder X-ray diffraction (PXRD) patterns show that UiO-66 and Pd/UiO-66 match the simulated pattern of the MOF (Figure S1A), indicating the MOF structure is maintained after the loading of Pd NPs (2 wt%). The Brunauer-Emmett-Teller (B.E.T.) surface areas of UiO-66 before and after loading Pd are 1800 and 1530 $m^2 \cdot g^{-1}$, respectively (Figure S1C and Table S1). The micropore volume of UiO-66 also decreases slightly from 0.50 to 0.46 $cm^3 \cdot g^{-1}$. X-ray diffraction peaks of Pd NPs were not obvious, possibly due to the low metal loading. As shown in the TEM images (Figure S1B), the Pd NPs are dispersed uniformly mostly on the external surface of UiO-66 with an average diameter of 4.2 ± 0.7 nm. Kinetic studies revealed that the catalytic activity of UiO-66 in the Claisen-Schmidt condensation reaction only slightly decreased after loading Pd NPs.

The production of PQ or PTHQ can be achieved *via* cyclization after reduction of $–NO_2$ in ***4***. The cyclization can proceed in four possible paths (Scheme 2): (I) condensation of $–NH_2$ and C=O to form PQ as the direct key intermediate; (II) condensation of $–NH_2$ and –OH *via* nuclear substitution to form intermediate 2-phenyl-1,2-dihydroquinoline after reduction of C=O; (III) condensation of $–NH_2$ and C=O to intermediate 2-phenyl-1,2-dihydroquinoline after reduction of C=C; and (IV) condensation of $–NH_2$ and –OH *via* nuclear substitution to form PTHQ directly after reduction of both C=C and C=O.

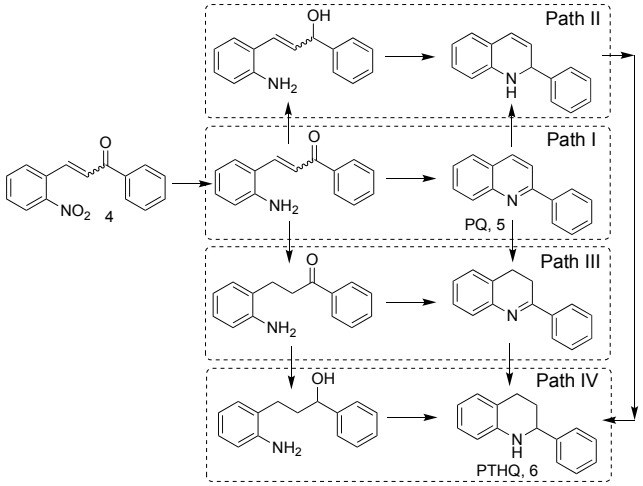

Scheme 2. Reductive cyclization of ***4*** to PTHQ catalyzed by Pd/UiO-66, showing four possible cyclization paths. Possible reactant H_2 and product H_2O are omitted.

Before carrying out the one-pot tandem synthesis of PTHQ from NBA and ACP (discussed in a latter section), we conducted reductive cyclization (Step 2) of ***4*** which was isolated from the condensation reaction mixture (Step 1). Their concentration profiles follow pseudo-first-order rate law when the hydrogen gas is of large excess and catalyst concentration remains unchanged; therefore, the results are presented as normalized concentrations in Figure 2.[30] The conversion of ***4*** was completed in 5 h with 56% yield to PTHQ at 40 °C under 27.6 bar H_2, Figure 2A. PQ is also formed from ***4*** (Figure 2A), reaching maximal yields of 23% at 2 h. To determine whether the hydrogenation of PQ is the major reaction path to PTHQ, we tested the hydrogenation of PQ under the same conditions. The PTHQ production from PQ was significantly slower than that from ***4,*** Figure 2B. These results suggest that PQ is a side product rather than the rate-limiting intermediate toward PTHQ, which is also confirmed by the hydrogenation of ***4*** and PQ under ambient-pressure H_2 at 50 °C, Figure S3. Furthermore, there is a mass loss with ***4*** as the reactant, which cannot be accounted for with any peaks in gas chromatograms.

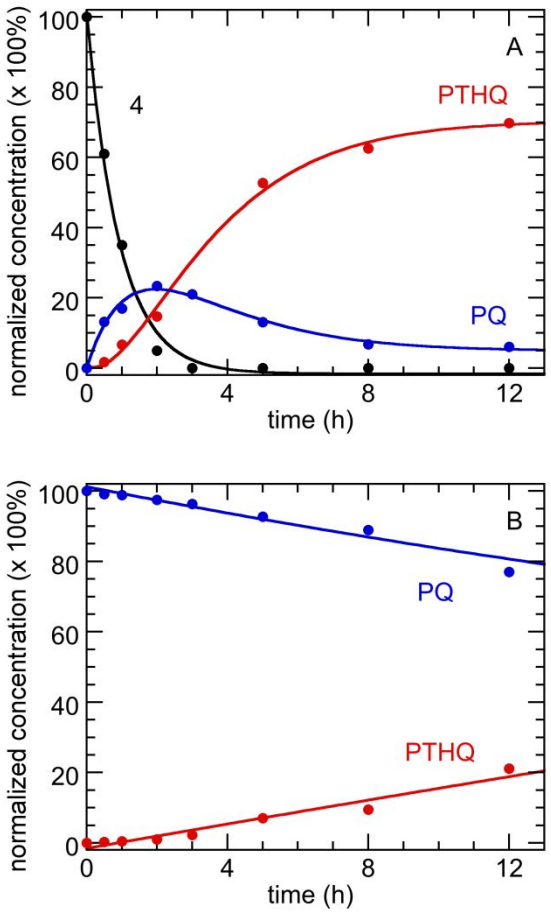

Figure 2. Time-resolved concentration profiles of Pd/UiO-66 catalyzed hydrogenation reaction of (A) *4* and (B) PQ at 40 °C and 27.6 bar H_2. Reaction conditions: substrate (0.2 mmol), 2 wt% Pd/UiO-66 (5 mg, ~ 0.5 mmol% Pd), solvent toluene (2 mL). Conversions were calculated based on analysis of GC results. The lines are added to guide the eye.

Mechanistic study with *operando* MAS-NMR To further maximize production of PQ or PTHQ, it is crucial to understand the reaction network leading to their formation, which is not obvious based on *ex situ* studies. Previous works by Crabtree[31] and Soós[32] used spectroscopic and DFT methods for the simple reduction of quinolines to THQs using homogeneous catalysts. Similar approaches cannot be readily applied to heterogeneous catalytic systems due to the complexity of the molecular transformation in our multiphasic reaction systems. Therefore, we employed *operando* high-pressure MAS-NMR studies to explore the reaction network.

The high-pressure MAS rotor[33,34] was loaded with ACP, NBA (0.83 equiv.) and Pd/UiO-66 in toluene. The ACP was isotopically labeled at both a- and b- positions with ^{13}C (194.5 and 24.3 ppm, respectively), allowing fast-tracking of molecular evolution with ^{13}C NMR. Therefore, each intermediate and product was detected as two doublets due to $^1J_{CC}$ while the non-labeled positions remained invisible. To avoid any possible influence of unreacted ACP on mechanistic study, ^{13}C-labelled ACP was added only in a slight excess.

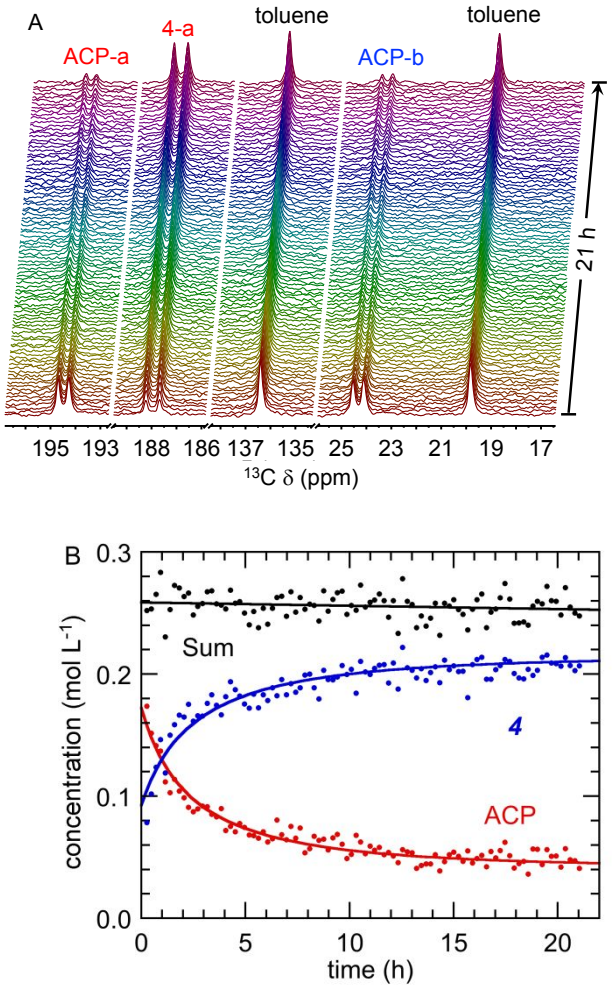

Figure 3. Claisen-Schmidt condensation reaction of ACP and NBA at 80 °C. (a) Arrays of direct polarization ^{13}C MAS-NMR spectra (MAS rate: 5 kHz, 8 scans per transient); (b) kinetic analysis of time-resolved NMR spectra. The 5 mm NMR rotor was loaded with ACP-α,β-$^{13}C_2$ (1.56 mg, 12.8 μmol) and NBA (1.61 mg, 10.7 μmol) in 50 μL toluene with 1 wt% Pd/UiO-66 (1 mg). The curvefits (solid lines) were obtained by fitting the second-order rate equation.

In Step 1, the Claisen-Schmidt condensation was conducted under air at 80 °C (Figure 3A). The ACP resonances started to decrease in intensity with the appearance of two new doublets at 187.4 and 126.5 ppm (Figures 3A and S4), assigned to ***4***. A trace amount of β-hydroxyketone intermediate ***3*** was detected when lowering the reaction temperature to 60 °C, Figure S5. No aldol product was observed between two acetophenone molecules at both tested temperatures. At 12 h, the yield of ***4*** was 80% based on ACP, and the selectivity was >99%; besides, the total concentration stayed constant after 21 h. The concentration profiles of ACP and ***4*** were extracted from the NMR arrays acquired at 80 °C (Figure 3A). The

time-resolved data of ACP and ***4*** were curve-fitted with second-order rate equations,[35] Figure 3B. The pseudo-second-order rate constants of ACP and compound ***4*** were almost identical: 2.7 ± 0.1 M^{-1} h^{-1} and 2.6 ± 0.2 M^{-1} h^{-1}, respectively.

In Step 2, the rotor, further charged with 27.6 bar H_2, was heated to 40 °C and maintained for 22 h. The high pressure of H_2 gas ensured a large excess of H_2 (ca. 15× of ***4*** by mol). Resonances of ***4*** disappeared after 2 h with the appearance of several sets of doublets, Figure 4. PTHQ (55.1 and 30.1 ppm) and PQ (155.7 and 117.2 ppm) were observed as expected products. Two doublets at 195.7 and 37.9 ppm are assigned to the a and b carbons in ***7***, arising from the reduction of the C=C in ***4***, Scheme 3. The chemical shift of ***7*** is confirmed with an authentic sample of ***7*** (Supporting information).

A new resonance at 121.4 ppm instantly appeared in the first spectrum and disappeared within 2 hours, following which an adjacent signal at 120.0 ppm first formed and then disappeared. Pairing signals of these two new resonances (121.4 and 120.0 ppm) also partially overlap with ***4***-a (187.6 ppm), indicating the two new species preserve both C=O and C=C functionalities. The lower frequencies of the b carbons of these two new species are mostly due to the reduction of the $–NO_2$ group in ***4***. Therefore, we can most likely assign the new peaks to ***8*** containing hydroxylamine and ***9*** with amine (Scheme 3). Compound ***8*** is an unstable molecule, and its *in situ* observation (up to 0.04 mol L^{-1}) is seldom reported. Few reports on the detection of phenylhydroxyamine are available with *in situ* and *ex situ* NMR but not under pressurized H_2.[36,37] The detections were only reported with *in situ* IR spectroscopy under pressure (10 bar H_2),[38,39] but its quantification was not achieved. The formation of stable products and intermediates, PTHQ, PQ, ***4***, ***7***, and ***9***, was also confirmed by *ex situ* HPLC-MS analysis of samples taken from a batch reactor after 30 min operating at 27.6 bar and 40 °C, Figure S6.

Compound ***11***, the further hydrogenation intermediate from either ***7*** or ***9***, cannot be identified in the NMR spectra, nor detected by either GC-MS or HPLC-MS. The absence of ***11*** is possibly due to its low concentration as it readily cyclizes. However, the detection of ***7*** can indirectly prove the existence of ***11*** as a short-lived intermediate. The carbonyl signals of ***4***, ***7***, ***8***, and ***9*** drift slightly to lower frequency, mostly due to the interaction of their carbonyls with side-product water.

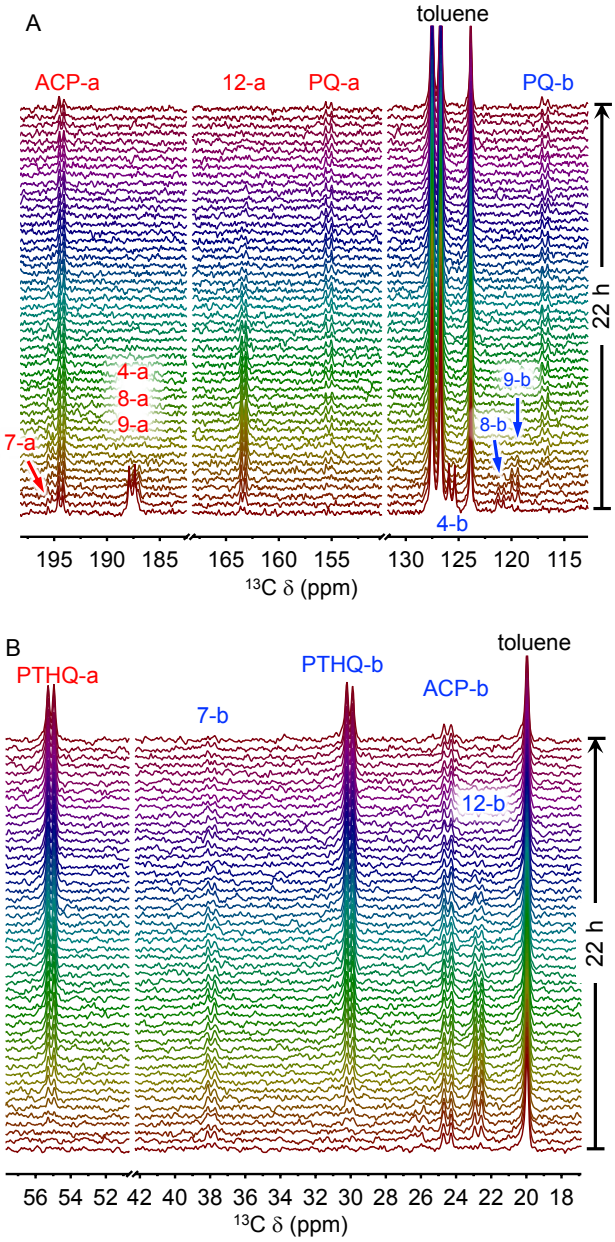

Figure 4. Arrays of direct polarization ^{13}C MAS-NMR spectra (8 scans per transient), recorded during reductive cyclization of ***4*** at 40 °C under 27.6 bar H_2, showing (A) 198 - 113 ppm and (B) 58 - 17 ppm. The 5 mm NMR rotor, containing the reaction mixture after Claisen-Schmidt condensation, was pressurized with H_2 at 22 °C. MAS rate: 5 kHz.

In Figure 4, there is another set of two pronounced doublets (163.7 and 22.7 ppm), which presumably can be assigned to 2-phenyl-3,4-dihydroquinoline (***12,*** in Path III, Scheme 2), agreeing with the literature results.[40] Compound ***12*** cannot be detected by traditional chromatographic techniques,[40] including TLC (Figure S7), GC-MS, or HPLC-MS, most likely due to its instability. Surprisingly, our *operando* NMR result shows the maximal concentration of compound ***12*** is as high as 0.11 mol L^{-1} at 4 h. The direct identification of ***12*** was only once

reported, but not quantified, during the direct hydrogenation of quinones catalyzed by homogeneous Ru complex, using ESI-HRMS.[40] This further demonstrates the unique capability of *operando* MAS-NMR in detection and quantification of reactive intermediates to construct complex reaction networks, while *ex situ* methods can only provide insufficient or even misleading information.

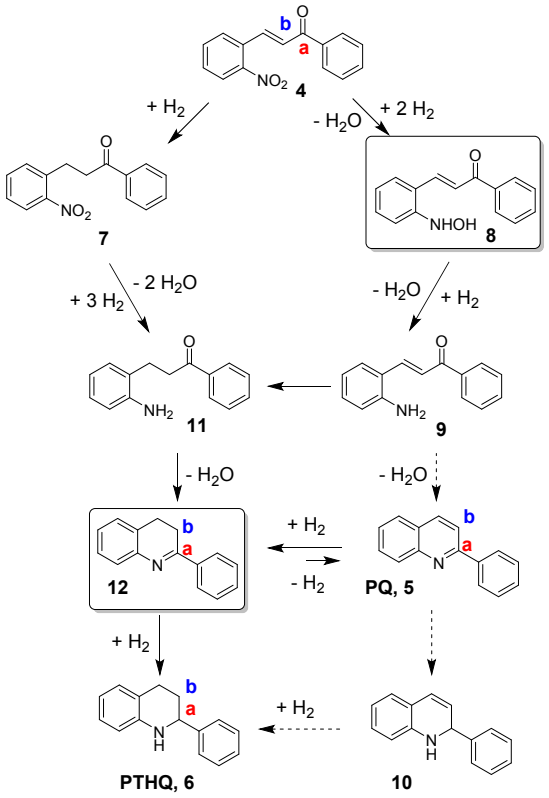

Scheme 3. Reaction networks of the Pd/UiO-66 catalyzed hydrogenation of *4* for the synthesis of *6*, as demonstrated by the NMR study. Molecules in solid box are unstable reaction intermediates. Solid lines represent transformations identified from experimental evidence. Dotted lines represent other possible transformations.

Compound ***12*** can be formed either by intramolecular condensation reaction of ***11*** or partial reduction of PQ, Scheme 3. The latter is rather unlikely under the reaction condition because the maximal concentration of PQ, 0.02 mol L^{-1} (yield: 8 %), was reached at 7 h, and further conversion of PQ was not clearly observed, Figure S8. Besides, all species before cyclization (***4***, ***7***, ***8***, and ***9***) were almost consumed when ***12*** peaked, indicating unobserved compound ***11*** is the major source of ***12***, Figure S8. The concentration of PTHQ and ***12*** together with the sum of ***4***+***7***+***8***+***9*** are shown in Figure 5. The rate constant of ***12*** consumption (0.18 ± 0.01 M^{-1} h^{-1}) matches well with that of PTHQ production (0.16 ± 0.01 M^{-1} h^{-1}), obtained by curvefitting according to a consecutive reaction kinetics with two pseudo first-order reactions, which strongly suggests that PTHQ is mostly derived from ***12***. The complete network of the reductive cyclization, based on *operando* NMR identified intermediates, is thus demonstrated in Scheme 3.

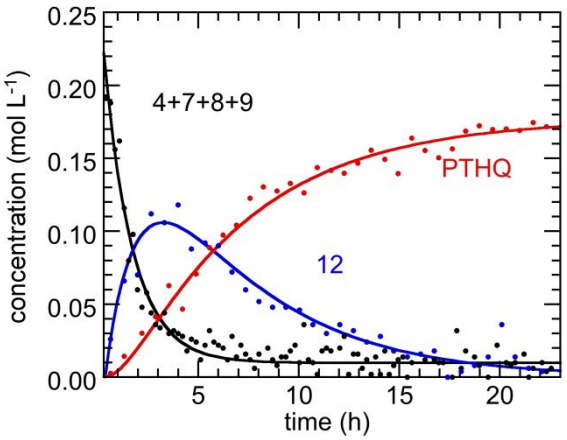

Figure 5. Concentration profiles of ***12***, PTHQ, and sum of ***4***, ***7***, ***8***, and ***9***, extracted from MAS-NMR arrays (Figure 4). For better presentation, only every 3rd data point is shown for all curves except the sum of ***4***, ***7***, ***8***, and ***9***. The concentration profiles of PTHQ and ***12*** were analyzed with biexponential rate equations. The other line is added only to guide the eye.

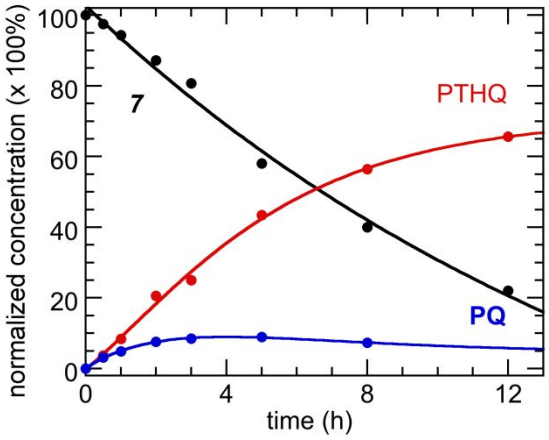

Figure 6. Time-resolved concentration profiles of Pd/UiO-66 catalyzed hydrogenation reaction of ***7*** at 40 °C and 27.6 bar H_2. Reaction conditions: ***7*** (0.2 mmol), 2 wt% Pd/UiO-66 (5 mg, ~ 0.5 mmol% Pd), solvent toluene (2 mL). Conversions were calculated based on analysis of GC results. The lines are added only to guide the eye.

To better benchmark the relative rates of hydrogenation, experiments starting with identified intermediate ***7***, in comparison to ***4*** and PQ, were also conducted under two conditions, 40 °C with 27.6 bar H_2 (Figure 6) and 50 °C with ambient H_2 (Figure S3). Under both conditions, the reaction of ***7*** is slower than compound ***4*** but faster than PQ, because ***4*** can be converted through two subsequent pathways (to ***7*** and ***8***), Scheme 3. The rate of PTHQ production from ***4*** and ***7*** (Figures 2A and 6) is almost identical. Besides, the concentration build-up was clearly observed for ***12*** but

not for ***11***. Together, these results suggest the turnover-limiting step is most likely the hydrogenation of ***12***. PQ cannot be directly produced from ***9*** because ***9*** preserves the trans-configuration of corresponding starting material ***4*** with a large $^3J_{HH}$ coupling constant (15.5 Hz) of the olefinic protons. Therefore, PQ is yielded as a result of the Pd/UiO-66 catalyzed dehydrogenation of ***12***. Similar dehydrogenation reactions have been reported as an equilibrium enabled by Pd-based catalysts for reversible hydrogen storage.[41] The hydrogenation of ***12*** to PTHQ is faster than the dehydrogenation of ***12*** to PQ in the presence of H_2.

The mechanistic study clearly shows that Pd/UiO-66 can selectively favor the PTHQ formation pathway with a lower activation barrier, suggesting the advantage in using the reductive intramolecular cyclization reaction, when compared to the direct reduction of PQ. It should be noted that the full conversion of PQ to PTHQ *via* ***12*** can be achieved but under more forcing conditions (i.e., higher temperature).

Selective production of PQ over PHTQ The identification of reactive intermediates, i.e. ***12***, allows us the ability of switching the product selectively from PTHQ to PQ, by selectively enhancing the dehydrogenation of ***12*** to PQ. We employed two phosphoric acids as homogeneous transfer hydrogenation catalysts (Scheme 4), P1 with two phenyls and P2 with an octahydro-BINOL derivative. P1 and P2 have been widely applied in transfer hydrogenation reactions with Hantzsch ester as the hydrogen sources.[42,43] More importantly, both P1 and P2 are inert in H_2 activation[44-46] and phosphoric acids do not affect the structures and activity of Pd nanoparticles for hydrogenation reactions,[47] particularly when accessibility of acid center in P2 is protected by sterically-restricting neighboring group.[48] Using the same reaction condition in the MAS-NMR study, all reactions initiating with ***4*** reached 100% conversion in 19 h with or without the use of co-catalysts, Table 1.

Without any co-catalyst, **4** converted to PTHQ in high yield with only 1% of PQ (Table 1, entry 1); nevertheless, higher selectivity toward PQ (9%) was observed after adding 2 mol% P1 (Table 1, entry 2). Changing the co-catalyst to P2 (2 and 20 mol%) shifts the product selectivity more obviously, increasing the yield of PQ to 24% and 71%, respectively (Table 1, entries 3 and 4). It should be noted that the 71% yield of PQ was achieved under 27.6 bar H_2 in the presence of Pd. Furthermore, reactions starting with PTHQ did not yield PQ (Table 1, entries 5 and 6), suggesting PQ is solely generated from ***12*** in the presence of the co-catalyst. The success in the mechanism-inspired switch of the products on demand provides us an extra measure to achieve selective synthesis which further demonstrates the importance of a molecular-level understanding of reaction network in catalysis.

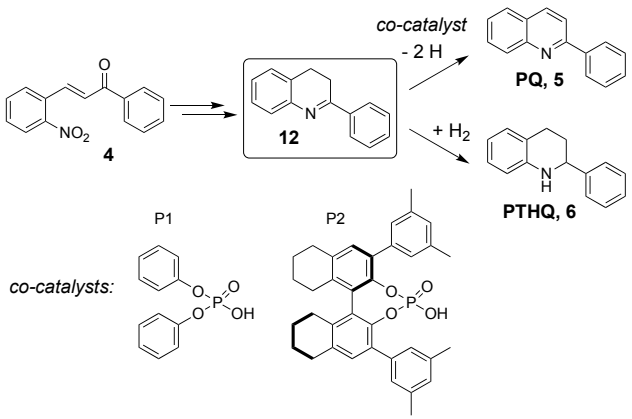

Scheme 4. Hydrogenation of ***4*** with and without P1 and P2 co-catalyst.

Table 1. Hydrogenation of different substrates catalyzed by Pd/UiO-66 with and without co-catalysts[a]

entry	substrates	co-catalyst	amount mol%	yield (%)[b]	
				PTHQ	PQ
1	4	–	–	95	1
2	4	P1	2	82	9
3	4	P2	2	70	24
4	4	P2	20	23	71
5	PTHQ	–	–	–	≤1
6	PTHQ	P2	20	–	≤1

[a] Reaction conditions: (1) ***4*** (0.1 mmol), 2 wt% Pd/UiO-66 (5 mg), toluene (1 mL), 40 °C, 27.6 bar H_2, 19 h [b] All yields are calculated by GC with mesitylene as the internal standard.

CONCLUSION

In conclusion, we have employed *operando* high-pressure MAS-NMR spectroscopy to construct the reaction network and achieve product selectivity in the synthesis of PTHQ and PQ. An acidic MOF-supported Pd NPs (Pd/UiO-66) as a bifunctional catalyst is used to achieve the one-pot tandem synthesis. The acidic sites in UiO-66 were efficient in catalyzing the Claisen-Schmidt condensation between NBA and ACP, and the *in situ* formed *ortho*-nitrochalcone was reduced multi-stepwise by the supported Pd NPs under H_2, generating PTHQs in moderate to high isolated yields. Multiple stable and unstable intermediates were pinpointed and quantified under the *operando* condition, which allows the clear elucidation of the conversion pathways under 27.6 bar H_2. The mechanistic insights not only demonstrate a catalyst-enabled route for efficient chemical transformation under milder conditions but also allow us to selectively produce

PQ or PTHQ *via* kinetic control of the conversion of the *in situ* observed key intermediate (***12***) employing a homogeneous co-catalyst in addition to heterogeneous Pd/UiO-66. The demonstrated methodology, i.e., mechanistic study-guided design of catalytic systems, can be well applied to other tandem reactions with complex reaction network involving multi-step interconnected transformations of various functional groups.

ASSOCIATED CONTENT

Supporting Information

Supporting Information is available free of charge on the ACS Publications website. Examples for the synthesis of PTHQs and PQs, structural characterization of catalysts (physisorption and XRD), additional *ex situ* reactivity results, *operando* NMR and related analysis, and characterization of reaction species. (PDF)

AUTHOR INFORMATION

Corresponding Author

*lqi@iastate.edu

*zhiguo.zhang@zju.edu.cn

*whuang@iastate.edu

ORCID

Long Qi: 0000-0002-1213-2946

Zhiguo Zhang: 0000-0003-1681-4853

Wenyu Huang: 0000-0003-2327-7259

Author Contributions

‡ These authors contributed equally.

Notes

The authors declare no competing financial interest.

Funding Sources

J.C., Z.B., Q.Y., Q.R. and Z.Z. are grateful for financial support from the National Key R&D Program of China (2016YFA0202900), the National Natural Science Foundation of China (21878266, 21722609). J. Chen thanks Zhejiang University for financial support. We thank the support from Iowa State University. L.Q. and T.K. are supported by the U.S. Department of Energy (DOE), Office of Basic Energy Sciences, Division of Chemical Sciences, Geosciences, and Biosciences. The Ames Laboratory is operated for the U.S. DOE by Iowa State University under Contract No. DE-AC02-07CH11358. W.H. appreciate the support from National Science Foundation (NSF) grant CHE-1566445.

ACKNOWLEDGMENT

We thank Gordon J. Miller for the use of the XRD instrument.

ABBREVIATIONS

NMR, nuclear magnetic resonance; HPLC, high-performance liquid chromatography; ESI-HRMS, electro-spray ionization high-resolution mass spectrometry; TLC, thin layer chromatography.

REFERENCES

(1) Huang, Y.-B.; Liang, J.; Wang, X.-S.; Cao, R. Multifunctional Metal–Organic Framework Catalysts: Synergistic Catalysis and Tandem Reactions. *Chem. Soc. Rev.* **2017,** *46*, 126-157.

(2) Li, X.; Zhang, B.; Tang, L.; Goh, T. W.; Qi, S.; Volkov, A.; Pei, Y.; Qi, Z.; Tsung, C.-K.; Stanley, L.; Huang, W. Cooperative Multifunctional Catalysts for Nitrone Synthesis: Platinum Nanoclusters in Amine-Functionalized Metal–Organic Frameworks. *Angew. Chem., Int. Edit.* **2017,** *56*, 16371-16375.

(3) Hunger, M.; Weitkamp, J. In Situ IR, NMR, EPR, and UV/Vis Spectroscopy: Tools for New Insight into the Mechanisms of Heterogeneous Catalysis. **2001,** *40*, 2954-2971.

(4) Qi, L.; Alamillo, R.; Elliott, W.; Andersen, A.; Hoyt, D.; Walter, E.; Sung Han, K.; Washton, N.; M Rioux, R.; A Dumesic, J.; L Scott, S.; Walter, E.; Kee; Han, S. Operando Solid-State NMR Observation of Solvent-Mediated Adsorption-Reaction of Carbohydrates in Zeolites. *ACS Catal.* **2017,** *7*, 3489-3500.

(5) Qi, L.; Chamas, A.; Jones, Z. R.; Walter, E. D.; Hoyt, D. W.; Washton, N. M.; Scott, S. L. Unraveling the Dynamic Network in the Reactions of an Alkyl Aryl Ether Catalyzed by Ni/ γ -Al_2O_3 in 2-Propanol. *J. Am. Chem. Soc.* **2019,** *141*, 17370-17381.

(6) Katritzky, A. R.; Rachwal, S.; Rachwal, B. Recent Progress in the Synthesis of 1,2,3,4-Tetrahydroquinolines. *Tetrahedron* **1996,** *52*, 15031-15070.

(7) Salas, P. F.; Herrmann, C.; Orvig, C. Metalloantimalarials. *Chem. Rev.* **2013,** *113*, 3450-3492.

(8) Wiesner, J.; Ortmann, R.; Jomaa, H.; Schlitzer, M. New Antimalarial Drugs. *Angew. Chem., Int. Edit.* **2003,** *42*, 5274-5293.

(9) Mukherjee, S.; Pal, M. Medicinal Chemistry of Quinolines as Emerging Anti-Inflammatory Agents: An Overview. *Curr. Med. Chem.* **2013,** *20*, 4386-4410.

(10) Zemtsova, M. N.; Zimichev, A. V.; Trakhtenberg, P. L.; Klimochkin, Y. N.; Leonova, M. V.; Balakhnin, S. M.; Bormotov, N. I.; Serova, O. A.; Belanov, E. F. Synthesis and Antiviral Activity of Several Quinoline Derivatives. *Pharm. Chem. J.* **2011,** *45*, 267-269.

(11) Solomon, V. R.; Lee, H. Quinoline as a Privileged Scaffold in Cancer Drug Discovery. *Curr. Med. Chem.* **2011,** *18*, 1488-1508.

(12) Afzal, O.; Kumar, S.; Haider, M. R.; Ali, M. R.; Kumar, R.; Jaggi, M.; Bawa, S. A Review on Anticancer Potential of Bioactive Heterocycle Quinoline. *Eur. J. Med. Chem.* **2015,** *97*, 871-910.

(13) Musiol, R. An Overview of Quinoline as a Privileged Scaffold in Cancer Drug Discovery. *Expert Opin. Drug. Dis.* **2017,** *12*, 583-597.

(14) Crabtree, R. H. Hydrogen Storage in Liquid Organic Heterocycles. *Energ Environ. Sci.* **2008,** *1*, 134-138.

(15) Sridharan, V.; Suryavanshi, P. A.; Menendez, J. C. Advances in the Chemistry of Tetrahydroquinolines. *Chem. Rev.* **2011,** *111*, 7157-7259.

(16) Scott, J. D.; Williams, R. M. Chemistry and Biology of the Tetrahydroisoquinoline Antitumor Antibiotics. *Chem. Rev.* **2002,** *102*, 1669-1730.

(17) Hu, Z.; Zhao, D. Metal-Organic Frameworks with Lewis Acidity: Synthesis, Characterization, and Catalytic Applications. *CrystEngComm* **2017,** *19*, 4066-4081.

(18) Hajek, J.; Vandichel, M.; Van de Voorde, B.; Bueken, B.; De Vos, D.; Waroquier, M.; Van Speybroeck, V. Mechanistic Studies of Aldol Condensations in UiO-66 and UiO-66-NH_2 Metal Organic Frameworks. *J. Catal.* **2015,** *331*, 1-12.

(19) Katz, M. J.; Mondloch, J. E.; Totten, R. K.; Park, J. K.; Nguyen, S. T.; Farha, O. K.; Hupp, J. T. Simple and Compelling Biomimetic

Metal-Organic Framework Catalyst for the Degradation of Nerve Agent Simulants. *Angew. Chem., Int. Edit.* **2014,** *53*, 497-501.

(20) Granadeiro, C. M.; Ribeiro, S. O.; Karmaoui, M.; Valenca, R.; Ribeiro, J. C.; De Castro, B.; Cunha-Silva, L.; Balula, S. S. Production of Ultra-Deep Sulfur-Free Diesels Using a Sustainable Catalytic System Based on UiO-66(Zr). *Chem. Commun.* **2015,** *51*, 13818-13821.

(21) Yang, Q.; Xu, Q.; Jiang, H. L. Metal-Organic Frameworks Meet Metal Nanoparticles: Synergistic Effect for Enhanced Catalysis. *Chem. Soc. Rev.* **2017,** *46*, 4774-4808.

(22) Chen, L.; Luque, R.; Li, Y. Controllable Design of Tunable Nanostructures inside Metal-Organic Frameworks. *Chem. Soc. Rev.* **2017,** *46*, 4614-4630.

(23) Rosler, C.; Fischer, R. A. Metal-Organic Frameworks as Hosts for Nanoparticles. *CrystEngComm* **2015,** *17*, 199-217.

(24) Dhakshinamoorthy, A.; Garcia, H. Cascade Reactions Catalyzed by Metal Organic Frameworks. *ChemSusChem* **2014,** *7*, 2392-2410.

(25) Jiang, J.; Yaghi, O. M. Brønsted Acidity in Metal–Organic Frameworks. *Chem. Rev.* **2015,** *115*, 6966-6997.

(26) Hajek, J.; Caratelli, C.; Demuynck, R.; De Wispelaere, K.; Vanduyfhuys, L.; Waroquier, M.; Van Speybroeck, V. On the Intrinsic Dynamic Nature of the Rigid UiO-66 Metal–Organic Framework. *Chem. Sci.* **2018,** *9*, 2723-2732.

(27) Hajek, J.; Bueken, B.; Waroquier, M.; De Vos, D.; Van Speybroeck, V. The Remarkable Amphoteric Nature of Defective UiO-66 in Catalytic Reactions. *ChemCatChem* **2017,** *9*, 2203-2210.

(28) Elena, P. M.; Jiří, Č. $[Cu_3(BTC)_2]$: A Metal–Organic Framework Catalyst for the Friedländer Reaction. *ChemCatChem* **2011,** *3*, 157-159.

(29) Li, X. L.; Guo, Z. Y.; Xiao, C. X.; Goh, T. W.; Tesfagaber, D.; Huang, W. Y. Tandem Catalysis by Palladium Nanoclusters Encapsulated in Metal-Organic Frameworks. *ACS Catal.* **2014,** *4*, 3490-3497.

(30) Davis, M. E.; Davis, R. J., *Fundamentals of Chemical Reaction Engineering*. Courier Corporation: 2012.

(31) Dobereiner, G. E.; Nova, A.; Schley, N. D.; Hazari, N.; Miller, S. J.; Eisenstein, O.; Crabtree, R. H. Iridium-Catalyzed Hydrogenation of *N*-Heterocyclic Compounds under Mild Conditions by an Outer-Sphere Pathway. *J. Am. Chem. Soc.* **2011,** *133*, 7547-7562.

(32) Erős, G.; Nagy, K.; Mehdi, H.; Pápai, I.; Nagy, P.; Király, P.; Tárkányi, G.; Soós, T. Catalytic Hydrogenation with Frustrated Lewis Pairs: Selectivity Achieved by Size-Exclusion Design of Lewis Acids. *Chem.—Eur. J.* **2012,** *18*, 574-585.

(33) Walter, E.; Qi, L.; Chamas, A.; Mehta, H.; Sears, J.; L Scott, S.; Hoyt, D. Operando MAS-NMR Reaction Studies at High Temperatures and Pressures. *J. Phys. Chem. C* **2018,** *122*, 8209-8215.

(34) Chamas, A.; Qi, L.; Mehta, H. S.; Sears, J. A.; Scott, S. L.; Walter, E. D.; Hoyt, D. W. High Temperature/Pressure MAS-NMRmr for the Study of Dynamic Processes in Mixed Phase Systems. *Magn. Reson. Imaging* **2019,** *56*, 37-44.

(35) Espenson, J. H., *Chemical Kinetics and Reaction Mechanisms*. McGraw-Hill New York: 1995; Vol. 102.

(36) Chen, G. X.; Xu, C. F.; Huang, X. Q.; Ye, J. Y.; Gu, L.; Li, G.; Tang, Z. C.; Wu, B. H.; Yang, H. Y.; Zhao, Z. P.; Zhou, Z. Y.; Fu, G.; Zheng, N. F. Interfacial Electronic Effects Control the Reaction Selectivity of Platinum Catalysts. *Nat. Mater.* **2016,** *15*, 564-571.

(37) Gao, Y. J.; Ma, D.; Wang, C. L.; Guan, J.; Bao, X. H. Reduced Graphene Oxide as a Catalyst for Hydrogenation of Nitrobenzene at Room Temperature. *Chem. Commun.* **2011,** *47*, 2432-2434.

(38) Richner, G.; van Bokhoven, J. A.; Neuhold, Y. M.; Makosch, M.; Hungerbuhler, K. In Situ Infrared Monitoring of the Solid/Liquid Catalyst Interface During the Three-Phase Hydrogenation of Nitrobenzene over Nanosized Au on TiO_2. *Phys. Chem. Chem. Phys.* **2011,** *13*, 12463-12471.

(39) Corma, A.; Concepcion, P.; Serna, P. A Different Reaction Pathway for the Reduction of Aromatic Nitro Compounds on Gold Catalysts. *Angew. Chem., Int. Edit.* **2007,** *46*, 7266-7269.

(40) Wang, T.; Zhuo, L.-G.; Li, Z.; Chen, F.; Ding, Z.; He, Y.; Fan, Q.-H.; Xiang, J.; Yu, Z.-X.; Chan, A. S. C. Highly Enantioselective Hydrogenation of Quinolines Using Phosphine-Free Chiral Cationic Ruthenium Catalysts: Scope, Mechanism, and Origin of Enantioselectivity. *J. Am. Chem. Soc.* **2011,** *133*, 9878-9891.

(41) Deraedt, C.; Ye, R.; Ralston, W. T.; Toste, F. D.; Somorjai, G. A. Dendrimer-Stabilized Metal Nanoparticles as Efficient Catalysts for Reversible Dehydrogenation/Hydrogenation of *N*-Heterocycles. *J. Am. Chem. Soc.* **2017,** *139*, 18084-18092.

(42) Rueping, M.; Theissmann, T.; Antonchick, A. P. Metal-Free Brønsted Acid Catalyzed Transfer Hydrogenation-New Organocatalytic Reduction of Quinolines. *Synlett* **2006**, 1071-1074.

(43) Rueping, M.; Theissmann, T.; Raja, S.; Bats, J. W. Asymmetric Counterion Pair Catalysis: An Enantioselective Brønsted Acid-Catalyzed Protonation. *Adv. Synth. Catal.* **2008,** *350*, 1001-1006.

(44) Fleischer, S.; Zhou, S.; Werkmeister, S.; Junge, K.; Beller, M. Cooperative Iron–Brønsted Acid Catalysis: Enantioselective Hydrogenation of Quinoxalines and 2 H-1,4-Benzoxazines. *Chem.—Eur. J.* **2013,** *19*, 4997-5003.

(45) Qin, J.; Chen, F.; He, Y.-M.; Fan, Q.-H. Asymmetric Hydrogenation of 3-Substituted 2*H*-1,4-Benzoxazines with Chiral Cationic Ru-MsDPEN Catalysts: A Remarkable Counteranion Effect. *Org. Chem. Front.* **2014,** *1*, 952-955.

(46) Chen, Q.-A.; Gao, K.; Duan, Y.; Ye, Z.-S.; Shi, L.; Yang, Y.; Zhou, Y.-G. Dihydrophenanthridine: A New and Easily Regenerable NAD(P)H Model for Biomimetic Asymmetric Hydrogenation. *J. Am. Chem. Soc.* **2012,** *134*, 2442-2448.

(47) Chase, Z. A.; Fulton, J. L.; Camaioni, D. M.; Mei, D.; Balasubramanian, M.; Pham, V.-T.; Zhao, C.; Weber, R. S.; Wang, Y.; Lercher, J. A. State of Supported Pd During Catalysis in Water. *J. Phys. Chem. C* **2013,** *117*, 17603-17612.

(48) Rueping, M.; Antonchick, A. P.; Theissmann, T. A Highly Enantioselective Brønsted Acid Catalyzed Cascade Reaction: Organocatalytic Transfer Hydrogenation of Quinolines and Their Application in the Synthesis of Alkaloids. *Angew. Chem., Int. Edit.* **2006,** *45*, 3683-3686.

Table of Contents